High stability electron field emitters made of nanocrystalline diamond coated carbon nanotubes

K. J. Sankaran, K. Srinivasu, K. C. Leou, N. H. Tai, and I. N. Lin

Citation: Applied Physics Letters **103**, 251601 (2013); doi: 10.1063/1.4850525
View online: http://dx.doi.org/10.1063/1.4850525
View Table of Contents: http://scitation.aip.org/content/aip/journal/apl/103/25?ver=pdfcov
Published by the AIP Publishing

High stability electron field emitters made of nanocrystalline diamond coated carbon nanotubes

K. J. Sankaran,[1] K. Srinivasu,[2] K. C. Leou,[2] N. H. Tai,[1,a)] and I. N. Lin[3,b)]
[1]*Department of Materials Science and Engineering, National Tsing-Hua University, Hsinchu 300, Taiwan*
[2]*Department of Engineering and System Science, National Tsing-Hua University, Hsinchu 300, Taiwan*
[3]*Department of Physics, Tamkang University, Tamsui 251, Taiwan*

(Received 14 October 2013; accepted 1 December 2013; published online 16 December 2013)

We report enhanced life-time stability for the electron field emitters prepared by coating nanocrystalline diamond (NCD) on carbon nanotubes (CNTs). Upon overcoming the problem of poor stability in CNTs, the NCD-CNTs exhibit excellent life-time stability of 250 min tested at different applied voltages of 600 and 900 V. In contrast, the life-time stability of CNTs is only 33 min even at relatively low voltage of 360 V and starts arcing at 400 V. Hence, the NCD-CNTs with improved life-time stability have great potential for the applications as cathodes in flat panel displays and microplasma display devices. © *2013 AIP Publishing LLC*.
[http://dx.doi.org/10.1063/1.4850525]

One dimensional (1D) nanostructures (nanowires, nanorods, nanotubes, etc.) have attracted a great deal of interest for both scientific fundamentals in nanoscience and potential applications in nanoscale systems, including various electronic and photonic nanodevices.[1–4] Since the documented discovery of carbon nanotubes (CNTs) in 1991 (Ref. 5) and the realization of their high aspect ratio and small tip radius of curvature, their excellent electrical and mechanical properties and chemical inertness enable them to be used as electron sources in devices ranging from flat-panel displays to electron microscopes.[6–9] However, the short life-time and the poor stability of the CNTs have been the major barriers averting their profitable viability.[10] The residual gases in the devices can damage the CNT tips after long time ion bombardment, degrading the electron field emission (EFE) properties.[11] To surmount this deficiency, CNTs have been combined with other field emitting materials by depositing thin films on CNTs,[12–15] decorating CNTs with nanoparticles,[16] or by making composites of CNTs.[17,18]

Diamond is well known to possess a series of excellent physical and chemical properties, thereby invoking it to be a strongly competing cold cathode materials for EFE applications.[19] Diamond has the most strongly bonded crystal structure, which backs the reason for diamond-based EFE devices to possibly operate with better life-time stability and reliability, and moreover, it does not suffer tip burn-out to the same degree as like CNT devices. Furthermore, diamond could be activated at high temperature or high power due to its high electrical breakdown field and high thermal conductivity; and these superior properties are highly advantageous to EFE devices. Based on the significant EFE properties of CNTs and diamond films, it will be interesting to integrate these two carbon nanomaterials to yield highly stable EFE characteristics. Many attempts have been made to couple diamond and CNTs.[14,15,20–22]

In the present work, nanocrystalline diamond (NCD) films on CNTs have been deposited using microwave plasma enhanced chemical vapor deposition (MPECVD) system and their EFE properties are investigated. The achieved EFE behavior is comparable to that of CNTs, demonstrating that these promising NCD coated CNTs with markedly superior life-time stability can be employed to enhance the quality of EFE devices. Additionally, the advantage of these NCD coated CNTs with better EFE properties on exciting Ar plasma in a device with parallel-plate configuration is also demonstrated.

The CNTs were grown on Si substrates, using CH_4 as carbon source and Ni nanoclusters as catalysts, in a thermal chemical vapor deposition process (900 °C, 30 min). The Ni nanoclusters were obtained from the thermal annealing (600 °C, 10 min) of a thin Ni coating (~5 nm) on a Si substrate. The CNTs were then scratched off from the Si substrates, thoroughly mixed with Ag paste in a weight ratio of 1:1 and screen printed on a glass substrate, followed by heat treatment at 400 °C for 30 min. Fig. 1(a) shows the field emission scanning electron microscopy (FESEM; JEOL-6500) image of CNTs (designated as "bare CNTs"). The NCD films were directly grown on the bare CNTs by using MPECVD system (2.45 GHz, 6 in. IPLAS-CYRANNUS-I, Troisdorf, Germany) in a Ar(49%)/H_2(50%)/CH_4(1%) plasma with a microwave power of 1300 W for 60 min. The pressure and the flow rate were maintained at 80 Torr and 100 sccm, respectively. No external heater was used to heat the substrate and the substrate temperature was in the range of 450–470 °C, which was due to plasma heating and was monitored by a thermocouple embedded in the stainless steel substrate holder. Thus, obtained samples were designated as "NCD-CNTs." Fig. 1(b) shows FESEM image of NCD-CNTs, which reveals that the NCD films are conformally coated on CNTs. It is to be noted that there was no nucleation or any other pretreatments carried out for CNTs prior to the synthesis of NCD films. The formation of C-H bonds due to the presence of atomic hydrogen in the plasma is considered as defect sites on the sp^2 network. The continued hydrogenation of the CNT walls will either result in clustering of sp^3 defects or it will increase the density of isolated sp^3-point defects. The sp^3 defects offer suitable sites for nucleation of carbon

a)Electronic mail: nhtai@mx.nthu.edu.tw
b)Electronic mail: inanlin@mail.tku.edu.tw

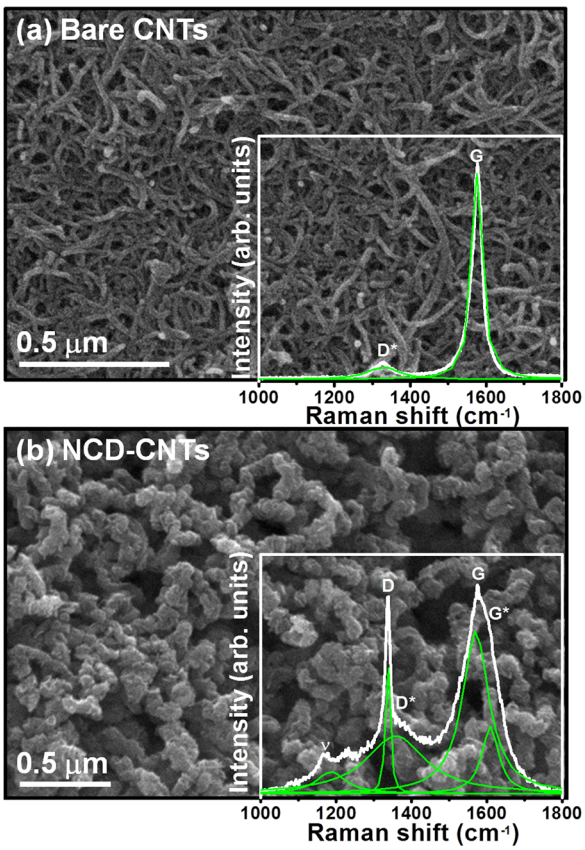

FIG. 1. FESEM micrographs for (a) bare CNTs and (b) NCD-CNTs with the insets showing the corresponding UV-Raman spectra.

nanoparticles. Initially, the nuclei forms an amorphous structure,[21] which then undergoes a phase transition into the diamond structure (crystallization).[23]

The insets of Figs. 1(a) and 1(b) show that the UV-Raman spectra (Lab Raman HR800, Jobin Yvon, λ: 325 nm) of bare CNTs and NCD-CNTs, respectively, indicating that while the CNTs contain predominantly the D*-band at 1328 cm^{-1} representing the presence of disordered sp^2 carbon[24] and G band at 1575 cm^{-1} representing the graphite phase, the NCD-CNTs contain broadened Raman peaks, which are characteristic of diamond materials with nano-sized grains. The UV-Raman spectra of the bare CNTs and the NCD-CNTs were deconvoluted by using the multi-peak Lorentzian fitting method. A sharp resonance peak near 1332 cm^{-1} (D-band) is observed, which represents sp^3-bonds, indicating the existence of diamond grains. Moreover, there is a ν-band at 1182 cm^{-1}, representing the presence of *trans*-polyacetylene phase at grain boundaries of NCD films[25] and D*-band at 1355 cm^{-1} representing the existence of disordered sp^2 carbon.[24] The G band of NCD films is observed at 1569 cm^{-1}. A shoulder peak around 1600 cm^{-1} (designated as G*-band) possibly arises from the nanographitic contents in the films.[26]

EFE is a kind of quantum tunneling in which electrons pass from the cathode to the anode through vacuum in the presence of a high electric field. The EFE properties of the bare CNTs and NCD-CNTs were measured with a tunable parallel plate setup, in which the cathode (bare CNTs or NCD-CNTs)-to-anode (molybdenum rod with a diameter of 2 mm) distance was controlled using a micrometer. The current-voltage (I-V) characteristics were measured using an electrometer (Keithley 2410) at pressure below 10^{-6} Torr. The EFE parameters were extracted from the obtained I-V curves by using Fowler-Nordheim (F-N) model[27]

$$J_e = \left(\frac{A\beta^2E^2}{\varphi}\right)\exp\left(-\frac{B\varnothing^{\frac{3}{2}}}{\beta E}\right), \quad (1)$$

where $A = 1.54 \times 10^{-6}$ A eV/V^2 and $B = 6.83 \times 10^9$ $eV^{-3/2}$ V/m, β is the field-enhancement factor, E is the applied field, J_e is the emission current density, and φ is the work function of the emitting materials. We have fabricated five NCD-CNTs or bare CNTs based cathodic devices which were tested in the same configuration at three places of each sample by keeping a constant anode to cathode distance. The data presented in Fig. 2 are the average of the EFE properties of five NCD-CNTs or bare CNTs based EFE cathodic devices. Curve I in Fig. 2(a) shows that the bare CNTs possess very good EFE properties, viz. the EFE process for the bare CNTs can be turned on at $(E_0)_{CNTs} = 1.44$ V/μm and achieve high $(J_e)_{CNTs} = 1.97$ mA/cm^2 at an applied field of 2.77 V/μm. However, as expected, the bare CNTs cannot last very long. Curve I in Fig. 2(b) shows that the bare CNTs can only last for 33 min at an applied voltage of 360 V. They

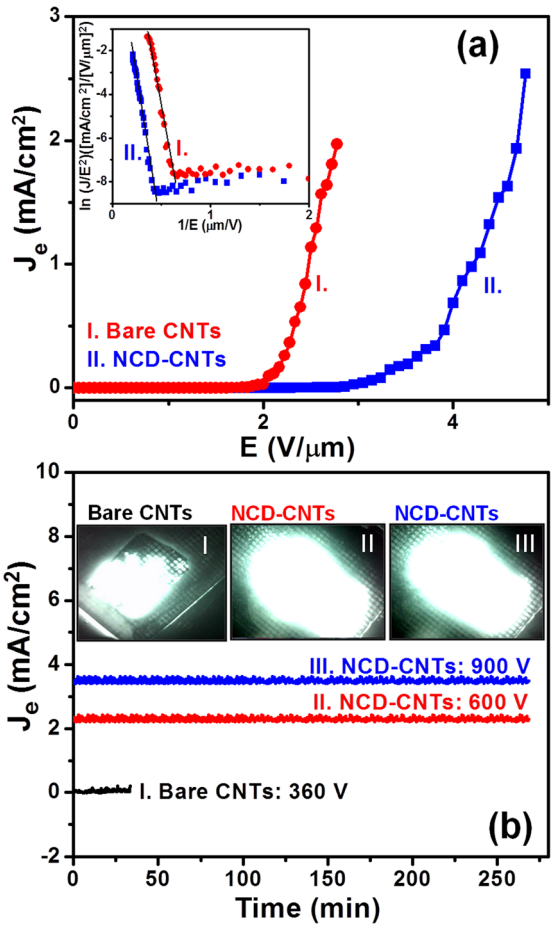

FIG. 2. (a) EFE current density (J_e) as a function of applied field (E) of bare CNTs and NCD-CNTs emitters (the inset shows the corresponding Fowler-Nordheim plots, i.e., $\log(J_e/E^2)$-$1/E$ plots), (b) life-time stability measurement, i.e., J_e versus time of (I) bare CNTs and (II, III) NCD-CNTs emitters with inset photographs showing the luminous field emission device with bare CNTs (or NCD-CNTs) as cathode at different applied voltages.

were completely burnt-out in a few seconds under the applied voltage of 400 V (figure not shown).

Curve II in Fig. 2(a) shows that the NCD-CNTs possess inferior EFE properties to the bare CNTs, which is as expected. The EFE process for NCD-CNTs can be turned on at $(E_0)_{\text{NCD-CNTs}} = 2.19\ \text{V}/\mu\text{m}$, which is markedly higher than $(E_0)_{\text{CNTs}}$. The J_e value of NCD-CNTs can only reach $(J_e)_{\text{NCD-CNTs}} = 0.006\ \text{mA/cm}^2$ at the applied field of 2.77 V/μm. It requires high applied field, $(E_0)_{\text{NCD-CNTs}} = 4.7\ \text{V}/\mu\text{m}$, to achieve the same EFE capacity (1.97 mA/cm^2) as that of the bare CNTs. The β values were estimated to be $(\beta)_{\text{CNTs}} = 4350$ and $(\beta)_{\text{NCD-CNTs}} = 2566$ for bare CNTs and NCD-CNTs, respectively. The NCD-CNTs exhibit significantly higher E_0 and lower J_e values that is apparently due to lower conductivity and smaller $\beta-$factor of the NCD-CNTs compared with the values of bare CNTs. Nevertheless, the coating of NCD on CNTs does provide a benefit for the EFE emitters, which is overwhelmingly advantageous for device applications, viz. it increases significantly the life-time of the emitters.

The J_e versus time curves of NCD-CNTs are presented in Fig. 2(b), which show the emission current variations recorded over a period of 250 min tested at different applied voltages of 600 and 900 V (curves II and III). As seen from the figure, there are no current degradations or notable fluctuations during this period. Moreover, EFE light emitting performance was tested using an indium tin oxide (ITO) coated glass on which green phosphor was coated, as anode and the bare CNTs (or NCD-CNTs) as cathode. The cathode-to-anode separation was fixed by a polytetrafluoroethylene (PTFE) spacer (1.0 mm in thickness). The uniformity of the emission current can be confirmed from the luminescence of the phosphor coated anode plate at the same applied voltages (600 and 900 V), which are shown in the insets II and III of Fig. 2(b), respectively. In contrast, the bare CNTs show an inhomogeneity in luminescence behavior [inset image I, Fig. 2(b)] at an applied voltage of 360 V. The luminescence image of the CNTs at the corresponding applied voltage of 360 V is the best luminescence available. When the applied voltage is increased to 400 V, the CNTs are completely burnt-out (figure not shown). This shows that the CNTs cannot withstand higher voltages.

To unravel the internal structure of the NCD-CNTs for understanding how the coating of NCD enhanced the life-time of the emitters, we used transmission electron microscopy (TEM; JEOL-2100F operated at 200 kV) to characterize the sample. The TEM image shown in Fig. 3(a) illustrates that several NCD particles with the sizes ranging from 2 to 70 nm were formed on the surface of the CNTs. The selected area electron diffraction (SAED) pattern of the NCD-CNTs is shown in the inset of Fig. 3(a). Ring-shaped patterns are observed. The diffraction rings correspond to the (111), (220) and (311) lattice planes of diamond. The (200) diffraction ring, which is a forbidden reflection in diamond lattice, is presumably arisen from *i-carbon*, the bcc structured allotrope of diamond, which are the nano-carbon clusters formed prior to the formation of the diamond nuclei. There is a prominent diffused ring at the center of the SAED pattern, signifying the existence of amorphous (or sp^2-bonded) phase. Fig. 3(b) shows the typical high resolution transmission electron microscopy (HRTEM) structure

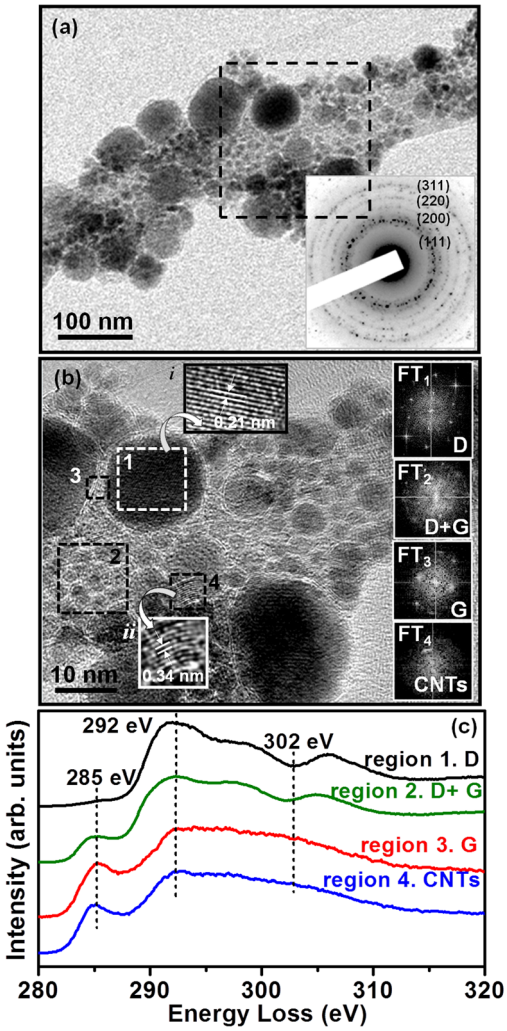

FIG. 3. (a) TEM micrograph for NCD-CNTs with the inset showing the SAED pattern and (b) HRTEM image of NCD-CNTs of the designated region in Fig. 3(a). High magnification HRTEM image "i" of the region "1" shows the diamond structure with a lattice spacing of 0.21 nm and HRTEM image "ii" of region "4" shows the CNT structure with a lattice spacing of 0.34 nm. Moreover, the insets Fourier-transformed diffractogram of the regions marked "1–4" in the HRTEM image are shown in the insets FT_1–FT_4, respectively, to illustrate the presence of diamond, graphite and CNT phases. (c) EELS spectra for the corresponding regions marked "1–4" in the HRTEM image [Fig. 3(b)].

image of the NCD-CNTs, corresponding to the designated region in Fig. 3(a). The Fourier transformed (FT_1) diffractogram corresponding to large aggregate in region "1" indicates clearly the diamond (D) phase that is more clearly revealed by the high magnification HRTEM image "*i*" of the region "1" presented in Fig. 3(b), illustrating the crystalline nature of diamond with a lattice spacing of 0.21 nm for the large aggregates. The FT_2 image of the region "2" shows a spotted diffraction pattern arranged in a ring, which corresponds to diamond (D) phase, and a diffused diffraction ring located at the center of the FT image, which corresponds to graphite (G) phase. Hence it is evident that the "small-cluster" contained nanosized diamond particles, which are surrounded by graphitic grain boundaries. To illustrate more clearly the grain boundary phases, the FT_3 image is taken from the region "3," which signifies the existence of graphitic phases in the grain boundaries of NCD particles, which is in accord with the UV-Raman spectroscopy

observation shown in the inset of Fig. 1(b). In addition, the FT_4 image corresponding to the marked region "4" illustrates the presence of CNTs, that is, again, revealed by the high magnification HRTEM image "*ii*" of the corresponding region "4," showing the CNT structure with the lattice spacing of 0.34 nm.

Electron energy loss spectroscopy (EELS) spectra were recorded in the carbon K-edge region to unambiguously distinguish between the different carbon materials such as diamond, graphite, and amorphous carbon.[28] Fig. 3(c) shows the EELS spectra for the corresponding regions "1–4" of Fig. 3(b). The EELS spectrum 1 for large aggregates in region "1" exhibits a sharp peak around 292.0 eV, corresponding to the transitions from the 1 s to the σ^* energy states (1 s-σ^*) and a dip around 302.0 eV, which is a characteristic feature of the crystalline diamond.[29] No signal near 284.5 eV (the Π^*-band) was observed, implying that there is no sp^2-bonded carbon contained in this large diamond aggregate. The spectrum 2 of region "2" corresponds to the signal for sp^3-bonded diamond with a shoulder band around 285.0 eV that confirms the presence of graphitic phases in the grain boundaries. Spectra 3 and 4 for regions "3" and "4," respectively, shows a band at 285.0 eV, which corresponds to the graphite phases (existing in the grain boundaries of NCD) and the CNTs.[29] No diamond signal is observed in these spectra. Hence, it is evident from the TEM and EELS studies, CNTs are conformally coated by NCD films and each nanosized diamond grain is surrounded by graphitic grain boundaries.

The beneficial effect of NCD coating on increasing the robustness of the CNTs can be better illustrated by using these EFE emitters as cathodes for a microplasma device, which is the harshest environment for electron emitters, as the emitters are subjected to energetic Ar-ions bombardment in these devices. The plasma illumination (PI) characteristics of a microplasma device using bare CNTs (or NCD-CNTs) as cathodes were investigated, in which the ITO coated glass was used as an anode. The cathode-to-anode separation was fixed by a PTFE spacer (1.0 mm in thickness). A circular hole about 8.0 mm in diameter was cut out in the PTFE spacer to form a microcavity. The plasma was triggered using a pulsed direct current voltage in a bipolar pulse mode (20 ms square pulse, 6 kHz repetition rate). The chamber was evacuated to reach a base pressure of 0.1 mTorr and was then purged with Ar for 10 min. The Ar gas was channeled into the chamber at a flow rate of 10 sccm throughout the measurements. The plasma current versus applied voltage was measured using an electrometer (Keithley 237). The data presented in Fig. 4 are the average of PI characteristics of tested NCD-CNTs or bare CNTs based microplasma cathodic devices which were tested in the same configuration. Fig. 4(a) shows the series of photographs of the PI behavior of the plasma devices, which utilized the bare CNTs [image series I, Fig. 4(a)] and NCD-CNTs [image series II, Fig. 4(a)] as cathode materials. The intensity of the plasma increases monotonically with the applied voltage. The bare-CNTs based microplasma devices need 320 V [$(E_{th})_{CNTs} = 0.32$ V/μm; image series I, Fig. 4(a)] to trigger the plasma, while the NCD-CNTs based microplasma devices can be triggered by a voltage = 330 V [$(E_{th})_{NCD\text{-}CNTs} = 0.33$ V/μm; image series II, Fig. 4(a)]. The PI characteristics are better

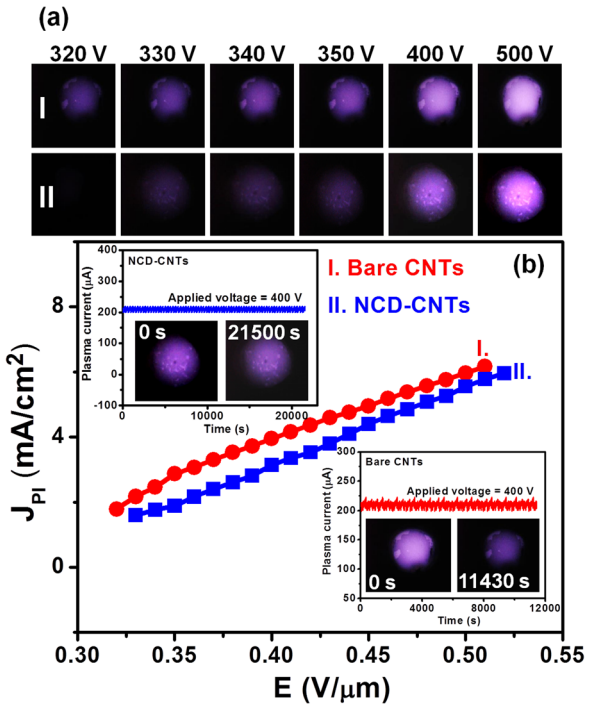

FIG. 4. (a) The photographs of plasma illumination characteristics and (b) plasma current density (J_{PI}) versus applied field (E) of a microplasma cavity, which utilized the ITO coated glass as anode and using either (I) bare CNTs or (II) NCD-CNTs as cathode materials. The upper left inset in Fig. 4(b) shows the plasma illumination stability of NCD-CNTs electrodes at 0 s and 360 min (21 500 s), whereas the bottom right inset shows the plasma illumination stability of bare CNTs electrodes at 0 s and 190 min (11 430 s), after ignition of plasma at the applied voltage of 400 V, revealing that the illumination of the NCD-CNTs plasma is essentially not degraded even after long time services.

illustrated by the variation of the plasma current density (J_{PI}) versus E, which is plotted in Fig. 4(b). The bare CNTs based microplasma devices [curve I of Fig. 4(b)] achieve a J_{PI} value of 6.1 mA/cm^2 at an applied field of 0.50 V/μm, whereas the J_{PI} reaches 5.9 mA/cm^2 at the same applied field for the devices which were electroded with NCD-CNTs [curve II of Fig. 4(b)].

To evaluate the stability of the CNTs and NCD-CNTs cathode materials, the plasma current was monitored over a long period with a constant applied voltage of 400 V [inset of Fig. 4(b)]. The plasma current of 210 μA decayed fast after 190 min (11 430 s) of plasma ignition for the bare CNTs-based microplasma devices [bottom right inset, Fig. 4(b)]. The intensity of the PI for the microplasma devices is reduced at 11 430 s as compared to the 0 s. In contrast, the plasma current of 210 μA is upheld for a period over 360 min (21 500 s), showing high life-time stability for NCD-CNTs based microplasma devices [upper left inset, Fig. 4(b)]. The intensity of the PI of the NCD-CNTs based microplasma devices at 400 V remains stable over 360 min (21 500 s) that represents the high stability of the NCD-CNTs. Apparently, the better PI performance of the microplasma devices based on the NCD-CNTs, as compared with bare CNTs-based ones, is intimately correlated with the superior robustness of NCD coated CNTs based electron field emitters. The microplasma based devices represent a photonics technology at the intersection of plasma science, optoelectronics, and materials science and provide a great potential for a broad spectrum of

applications in microdisplays, material synthesis, and elemental analysis.[30–32] Particularly, diamond exhibits a large secondary electron emission efficiency, which is especially proficient for serving as a cathode material in microplasma based devices.[33]

In conclusion, a facile and a reproducible way of synthesizing NCD films on CNTs with high life-time stability EFE and PI performances is being demonstrated. Surmounting the problems of CNTs electron field emitters, which acquire poor stability, the NCD-CNTs display excellent EFE life-time stability of 250 min tested at different applied voltages of 600 and 900 V. There are no notable current degradations or fluctuations of NCD-CNTs over a period of 250 min at different applied voltages of 600 and 900 V. In addition, the plasma current of 210 μA is upheld for a period over 360 min (21 500 s), showing better life-time plasma stability for NCD-CNTs based microplasma devices than that of bare CNTs (190 min). The present approach of synthesizing NCD-CNTs is a direct and simple process that provides a solution for the fabrication of functional 1D field emission devices and opens prospects of high definition flat panel displays or microplasma based devices.

The authors like to thank the financial support of National Science Council, Taiwan, through the Project Nos. NSC 101-2221-E-007-064-MY3 and NSC 101-2112-M-032-002-MY2.

[1]Y. Xia, P. Yang, Y. Sun, Y. Wu, B. Mayers, B. Gates, Y. Yin, F. Kim, and H. Yan, Adv. Mater. **15**, 353 (2003).
[2]J. Hao, Y. Lian, L. Guan, D. Yue, X. Guo, S. Zhao, Y. Zhao, K. Ibrahim, J. Wang, H. Qian, J. Dong, H. Yuan, G. Xing, and B. Sun, Nanoscale **3**, 3103 (2011).
[3]M. H. Huang, S. Mao, H. Feick, H. Q. Yan, Y. Y. Wu, H. Kind, E. Weber, R. Russo, and P. D. Yang, Science **292**, 1897 (2001).
[4]Y. Sun, Nanoscale **2**, 1626 (2010).
[5]S. Ijima, Nature **354**, 56 (1991).
[6]M. Bansal, R. Srivastava, C. Lal, M. N. Kamalasanan, and L. S. Tanwar, Nanoscale **1**, 317 (2009).
[7]W. A. deHeer, A. Chatelain, and D. Ugate, Science **270**, 1179 (1995).
[8]Q. Cao and S. Han, Nanoscale **5**, 8852 (2013).
[9]P. Castrucci, M. Scarselli, M. Crescenzi, M. Khakani, and F. Rosei, Nanoscale **2**, 1611 (2010).
[10]K. A. Dean, T. P. Burgin, and B. R. Chalamala, Appl. Phys. Lett. **79**, 1873 (2001).
[11]K. A. Dean and B. R. Chalamala, Appl. Phys. Lett. **75**, 3017 (1999).
[12]J. M. Green, L. Dong, T. Gutu, J. Jiao, J. F. Conley, and J. Y. Ono, J. Appl. Phys. **99**, 094308 (2006).
[13]R. K. Joshi, J. Engstler, A. Navitski, V. Sakharuk, G. Muller, and J. J. Schneider, Nanoscale **3**, 3258 (2011).
[14]Y. Zou, P. W. May, S. M. C. Vieira, and N. A. Fox, J. Appl. Phys. **112**, 044903 (2012).
[15]A. Fiori, S. Orlanducci, V. Sessa, E. Tamburri, F. Toschi, M. L. Terranova, A. Ciorba, M. Rossi, M. Lucci, and A. S. Barnard, J. Nanosci. Nanotechnol. **8**, 1989 (2008).
[16]D. H. Lee, J. A. Lee, W. J. Lee, D. S. Choi, W. J. Lee, and S. O. Kim, J. Phys. Chem. C **114**, 21184 (2010).
[17]J. M. Rosolen, S. Tronto, M. S. Marchesin, E. C. Almeida, N. G. Ferreira, C. H. Patrick Poá, and S. R. P. Silva, Appl. Phys. Lett. **88**, 083116 (2006).
[18]D. Varshney, M. Ahmadi, M. J. F. Guinel, B. R. Weiner, and G. Morell, Nanoscale Res. Lett. **7**, 535 (2012).
[19]K. J. Sankaran, H. C. Chen, B. Sundaravel, C. Y. Lee, N. H. Tai, and I. N. Lin, Appl. Phys. Lett. **102**, 061604 (2013).
[20]V. K. Rangari, G. M. Mohammad, S. Jeelani, Y. V. Butenko, and V. R. Dhanak, ACS Appl. Mater. Interfaces **2**, 1829 (2010).
[21]L. T. Sun, J. L. Gong, Z. Y. Zhu, D. Z. Zhu, S. X. He, Z. X. Wang, Y. Chen, and G. Hu, Appl. Phys. Lett. **84**, 2901 (2004).
[22]X. Xiao, J. W. Elam, S. Trasobares, O. Auceillo, and J. A. Carlisle, Adv. Mater. **17**, 1496 (2005).
[23]M. G. Fyta, I. N. Remediakis, and P. C. Kelires, Phys. Rev. B **67**, 035423 (2003).
[24]T. D. Corrigan, D. M. Gruen, A. R. Krauss, P. Zapol, and R. P. H. Chang, Diamond Relat. Mater. **11**, 43 (2002).
[25]K. J. Sankaran, N. Kumar, J. Kurian, R. Ramadoss, H. C. Chen, S. Dash, A. K. Tyagi, C. Y. Lee, N. H. Tai, and I. N. Lin, ACS Appl. Mater. Interfaces **5**, 3614 (2013).
[26]K. J. Sankaran, K. Panda, B. Sundaravel, H. C. Chen, I. N. Lin, C. Y. Lee, and N. H. Tai, ACS Appl. Mater. Interfaces **4**, 4169 (2012).
[27]R. H. Fowler and L. Nordheim, Proc. R. Soc. London, Ser. A **119**, 173 (1928).
[28]A. Dato, V. Radmilovic, Z. Lee, J. Philips, and M. Frenklach, Nano Lett. **8**, 2012 (2008).
[29]R. Arenal, P. Bruno, D. J. Miller, M. Bleuel, J. Lal, and D. M. Gruen, Phys. Rev. B **75**, 195431 (2007).
[30]J. G. Eden, S. J. Park, N. P. Ostrom, S. T. McCain, C. J. Wagner, B. A. Vojak, J. Chen, C. Liu, P. von Allmen, F. Zenhausern, D. J. Sadler, C. Jensen, D. L. Wilcox, and J. J. Ewing, J. Phys. D: Appl. Phys. **36**, 2869 (2003).
[31]S. J. Park, J. Chen, C. J. Wagner, N. P. Ostrom, C. Liu, and J. G. Eden, IEEE J. Sel. Top. Quantum Electron. **8**, 387 (2002).
[32]A. Michels, S. Tombrink, W. Vautz, M. Miclea, and J. Franzke, Spectrochim. Acta, Part B **62**, 1208 (2007).
[33]A. Stacey, S. Prawer, S. Rubanov, R. Ahkvlediani, S. Michaelson, and A. Hoffman, Appl. Phys. Lett. **95**, 262109 (2009).